

# The polarity dependent effect of gyroviscosity on the flow shear stabilized Rayleigh–Taylor instability and an application to the plasma focus

E. L. Ruden

*Air Force Research Laboratory, Directed Energy Directorate, Kirtland AFB, New Mexico 87117-5776*

(Received 2 July 2003; accepted 4 November 2003)

The linear dispersion relation is derived for modes of an isothermal finite Larmor radius incompressible plasma with an equilibrium density and horizontal fluid velocity varying with depth in a uniform gravitational field. The velocity and magnetic field are assumed parallel and transverse to the wave number, respectively. Stability criteria are derived and unstable growth rate diagrams plotted for the combined Rayleigh–Taylor/Kelvin–Helmholtz modes for two and three region piecewise uniform cases representing an accelerated plasma layer with sheared flow. The effect of gyroviscosity on wave numbers larger than a critical value is shown to differ if the direction of the magnetic field is reversed, all else being equal, being either stabilizing or destabilizing depending on direction. This implies an electrode polarity dependence for a magnetically accelerated plasma with sheared flow consistent with the observation that plasma foci generally have superior performance if the center conductor is the anode. Characteristic properties of the shocked plasma layer of a plasma focus during the accretion phase are inferred for use with the model. Given a plasma focus with a central anode, a maximum  $B_0 t$  product is derived for high wave number stability for a given current waveform, where  $B_0$  is the driving magnetic field magnitude and  $t$  is the current risetime. When combined with a recognized empirical scaling law for neutron yield optimized D<sub>2</sub> plasma foci, a maximum current for high wave number stability is implied independent of  $t$ . For a linearly rising current, for example, this is 2 MA. Strategies for mitigating the constraints are discussed, such as applying an exponentially increasing current waveform. This and other parametric relationships of the model may lead to designs with higher performance than would otherwise be possible for plasma foci and other devices such as flow shear stabilized Z-pinches. [DOI: 10.1063/1.1637608]

## I. INTRODUCTION

Having a sheared fluid velocity has long been recognized as a potential mitigating factor for the Rayleigh–Taylor (R–T) instability. Kuo<sup>1</sup> determined that all wave numbers parallel to the direction of a vertically sheared horizontal fluid velocity are stabilized for an incompressible fluid of infinite depth with density exponentially increasing with height provided  $g/\lambda s^2 < 2$ . Here, gravitational acceleration  $g$ ,  $e$ -fold density scale height  $\lambda$ , and the derivative of horizontal fluid velocity with reference to height  $s$  are assumed constant. This is a particularly interesting result in magneto-hydrodynamics (MHD) since, if the fluid is a plasma supported by a magnetic field orthogonal to the sheared flow, modes in the magnetic field direction are stable too.<sup>2</sup>

To represent a magnetically accelerated ideal MHD plasma with a rapid transition from the driving magnetic field to a plasma layer of finite thickness, such as in a Z pinch or plasma focus (PF), stability diagrams based on Goldstein's dispersion relation for an incompressible fluid in a gravitational field with height dependent density and unidirectional horizontal velocity<sup>3</sup> are already published for various piecewise uniform cases. These cases are for density increasing with height in two equal steps,<sup>4</sup> and for density increasing from zero to a constant value at a given height, and then either staying constant or dropping back to zero at a greater height.<sup>5</sup> The flow shear in these cases is confined to

the intermediate layer, thereby generalizing Taylor's treatment of a piecewise uniform case of the Kelvin–Helmholtz (K–H) instability which assumes density *decreases* with height.<sup>6,7</sup> In all cases where the density increases with height, only R–T modes within a range of wave numbers are stabilized by flow shear, below and above which modes are unstable. Various mechanisms are proposed in the above articles to improve the stability of the more problematic higher wave numbers (which generally have a higher growth rate). Of these, the effect of finite Larmor radius<sup>5</sup> (FLR) is the subject of this paper.

Thompson<sup>8</sup> derives an equation of motion for a plasma that couples ion orbital motion to plasma velocity component gradients. Roberts and Taylor<sup>9</sup> identify the coupling coefficient  $\nu$  as a type of viscosity. Despite the suggestive terminology, the mathematical form of this coupling is significantly different from that of kinematic (collisional) viscosity. Roberts and Taylor's subsequent example shows for example that, unlike kinematic viscosity, gyroviscosity stabilizes sufficiently high wave numbers by coupling to velocity component gradients resulting from the linear (first order) R–T perturbation itself. This suggests that a stronger effect may result from gyroviscous coupling to a much larger (zeroth order) pre-existing flow shear factor  $s$ , as defined most generally by Eqs. (74). Another significant difference is that the force density vector resulting from gyroviscosity is asym-

metric under the transform  $x \rightarrow -x$ , where  $x$  is the direction of acceleration.

We generalize Goldstein's dispersion relation in this paper by adding an isothermal FLR correction to the MHD stress tensor,<sup>10</sup> which generalizes Roberts and Taylor's expression to allow for spatial variation in gyroviscosity, and revisit the aforementioned piecewise uniform cases. Two simplified general cases are presented to investigate the coupled effects of gyroviscosity and sheared flow on the stability of an accelerated plasma layer. Both are motivated by interest in the stability of a flow sheared plasma layer of thickness  $2d$  accelerated by a magnetic field. In case I, only high wave number modes with  $k \gg (2d)^{-1}$  are considered, so the slab may be assumed to be semi-infinite. This most simplified (two region) case is presented since the effects of gyroviscosity are greatest in this regime. We show that the proper combination of sheared flow and gyroviscosity stabilizes this case for all wave numbers *provided*  $s < 0$ . Gyroviscosity actually negates most of the stabilizing effect of the flow shear in a broad range of wave numbers if  $s > 0$ . This is a direct consequence of the aforementioned  $x \rightarrow -x$  asymmetry. The effect of the thickness of the plasma layer and/or flow sheared region is considered in case II by introducing a second boundary distance  $2d$  from the first. This generalizes the published stability diagrams where gyroviscosity is neglected.<sup>4,5</sup> We see that the high wave number behavior of case I is retained but, as without gyroviscosity, wave numbers below a critical value are unstable. While case II provides a more complete representation of the combined R–T/K–H instability for an accelerated plasma layer, case I is analytically much simpler and, therefore, more clearly illustrates the effects of the coupling of gyroviscosity to flow shear. In particular, case I helps clarify the large wave number behavior of both interfaces of case II.

The theoretical results are applied to the dynamics of a generic PF-type device, for which flow shear within the accelerated layer is implicit. It is observed empirically that PF generally operate more efficiently if the central conductor is the anode.<sup>11</sup> This is consistent with the the aforementioned polarity dependence of the gyroviscous-flow shear coupling, although other explanations have been proposed.<sup>12</sup> For a PF with a central anode, critical scaling issues are revealed that may affect the performance of existing and future machines with higher energies and currents.

## II. MODEL

We assume a perfectly conducting isothermal  $z$  invariant plasma with a magnetic field of magnitude  $B$  in the  $\mathbf{z}$  direction, and a uniform gravitational field of magnitude  $g$  in the  $-\mathbf{x}$  direction.  $\mathbf{x}$ ,  $\mathbf{y}$ , and  $\mathbf{z}$  are the  $x$ ,  $y$ , and  $z$  directional unit vectors, respectively. For incompressible motion confined to the  $x$ – $y$  plane, the MHD equation of motion supplemented by the isothermal transverse contribution to the FLR stress tensor  $\mathbf{\Pi}$  given by Hazeltine and Meiss,<sup>10</sup> Chap. 6, Eq. (123), along with the equations of continuity and state are

$$\rho \frac{\partial}{\partial t} \mathbf{v} + \rho (\mathbf{v} \cdot \nabla) \mathbf{v} = -\nabla p^* - g \rho \mathbf{x} - \nabla \cdot \mathbf{\Pi}, \quad (1)$$

$$\Lambda_x \equiv -(\nabla \cdot \mathbf{\Pi}) \cdot \mathbf{x} = \frac{\partial}{\partial x} \left[ \nu \rho \left( \frac{\partial v_y}{\partial x} + \frac{\partial v_x}{\partial y} \right) \right] - \frac{\partial}{\partial y} \left[ \nu \rho \left( \frac{\partial v_x}{\partial x} - \frac{\partial v_y}{\partial y} \right) \right], \quad (2)$$

$$\Lambda_y \equiv -(\nabla \cdot \mathbf{\Pi}) \cdot \mathbf{y} = -\frac{\partial}{\partial y} \left[ \nu \rho \left( \frac{\partial v_y}{\partial x} + \frac{\partial v_x}{\partial y} \right) \right] - \frac{\partial}{\partial x} \left[ \nu \rho \left( \frac{\partial v_x}{\partial x} - \frac{\partial v_y}{\partial y} \right) \right],$$

$$p^* \equiv \frac{k_B T}{m_i} \rho + \frac{B^2}{2\mu_0}, \quad \nu = \frac{k_B T_i}{2ZeB}, \quad T \equiv (T_i + ZT_e), \quad (3)$$

$$\frac{\partial}{\partial t} \rho + \nabla \cdot (\rho \mathbf{v}) = 0, \quad \nabla \cdot \mathbf{v} = 0, \quad (4)$$

$\mathbf{v}$ ,  $\rho$ ,  $\Lambda$ ,  $m_i$ ,  $\mu_0$ ,  $k_B$ ,  $T_i$ ,  $T_e$ ,  $e$ , and  $Z$  are the fluid velocity, density, FLR force density vector, ion mass, free space permeability, Boltzmann constant, ion and electron temperature, elementary charge, and mean ionization level, respectively. The incompressibility assumption greatly simplifies the analysis, but limits the range of validity of the model, as discussed in Sec. VI.

The equilibrium state of interest has  $\mathbf{v} = v_{y0}(x)\mathbf{y}$ ,  $\rho = \rho_0(x)$ ,  $\mathbf{B} = B_0(x)\mathbf{z}$ , and  $\nu = \nu_0(x)$ . These comprise a time independent solution to the governing equations provided, from Eq. (1) and Eqs. (2),

$$p_0^*(x) = -\nu_0 \rho_0 \frac{\partial v_{y0}}{\partial x} - g \int_0^x \rho_0(x') dx' + \text{constant}. \quad (5)$$

We now linearize the governing equations assuming a first order perturbation from this equilibrium with  $\exp(i\omega t +iky)$  dependence. Equilibrium and first order components are represented by 0 and 1 subscripts, respectively,

$$i\rho_0 v_{x1}(\omega + kv_{y0}) = -\frac{\partial}{\partial x} p_1^* - g\rho_1 + \Lambda_{x1}, \quad (6)$$

$$i\rho_0 v_{y1}(\omega + kv_{y0}) + \rho_0 v_{x1} \frac{\partial v_{y0}}{\partial x} = -ikp_1^* + \Lambda_{y1},$$

$$\Lambda_{x1} = \frac{\partial}{\partial x} \left[ (\nu_0 \rho_1 + \rho_0 \nu_1) \frac{\partial v_{y0}}{\partial x} + \nu_0 \rho_0 \left( \frac{\partial v_{y1}}{\partial x} + ikv_{x1} \right) \right] - ik\nu_0 \rho_0 \left( \frac{\partial v_{x1}}{\partial x} - ikv_{y1} \right), \quad (7)$$

$$\Lambda_{y1} = -ik \left[ (\nu_0 \rho_1 + \rho_0 \nu_1) \frac{\partial v_{y0}}{\partial x} + \nu_0 \rho_0 \left( \frac{\partial v_{y1}}{\partial x} + ikv_{x1} \right) \right] - \frac{\partial}{\partial x} \left[ \nu_0 \rho_0 \left( \frac{\partial v_{x1}}{\partial x} - ikv_{y1} \right) \right],$$

$$p_1^* = \frac{k_B T}{m_i} \rho_1 - \left( \frac{k_B T_i}{2Ze} \right)^2 \frac{\nu_1}{\mu_0 \nu_0^3}, \quad (8)$$

$$i\rho_1(\omega + kv_{y0}) + v_{x1} \frac{\partial \rho_0}{\partial x} = 0, \quad (9)$$

$$ikv_{y1} + \frac{\partial v_{x1}}{\partial x} = 0. \tag{10}$$

Equation (8) and Eq. (9) result from Eqs. (3) and Eqs. (4), respectively, while Eq. (10) results from  $\nabla \cdot \mathbf{v} = 0$  alone. We have eliminated the explicit appearance of  $B$  terms in Eq. (8) in favor of  $T_i$  (constant) and  $\nu$  terms so that the latter may be treated as an independent parameter.

To obtain a dispersion relation,  $p_1^*$  is first eliminated between Eqs. (6) by solving both for  $\partial p_1^* / \partial x$  and equating. An expression for  $\nu_1$  is obtained by substituting  $p_1^*$  in the second of Eqs. (6) with the r.h.s. of Eq. (8) and solving for  $\nu_1$ .  $\rho_1$  and  $v_{y1}$  are then eliminated by solving Eq. (9) and Eq. (10) for these terms, respectively, and substituting elsewhere. The result is, without any further approximations or assumptions,

$$D \left[ (\rho_0 \omega^{*2} - 2k\nu_0 \omega^* D\rho_0) D \left( \frac{u}{\omega^*} \right) + 2k\rho_0(k^2\nu_0 u - (D\nu_0)Du - (i\nu_1)D\omega^*) \right] = \frac{k^2 g u}{\omega^*} D\rho_0 + 2k^3 \nu_0 \rho_0 Du + k^2 \rho_0 u \omega^*, \tag{11}$$

$$(i\nu_1) = \frac{-S}{(1-S)\rho_0 D\omega^*} \left[ \frac{\rho_0 \omega^{*2}}{k} D \left( \frac{u}{\omega^*} \right) - 2(Du)D(\nu_0 \rho_0) + \rho_0 \nu_0 (k^2 u - D^2 u) + \left( \frac{k k_B T}{m_i} + \nu_0 D\omega^* \right) \frac{u D\rho_0}{\omega^*} \right], \tag{12}$$

$$S \equiv \mu_0 \rho_0 \nu_0^3 \left( \frac{2Ze}{k_B T_i} \right)^2 \frac{D\omega^*}{k} = \frac{\beta_i m_i}{4ZeB_0} \frac{D\omega^*}{k}, \tag{13}$$

$$\beta_i \equiv \frac{\rho_0 k_B T_i / m_i}{B_0^2 / 2\mu_0}, \quad D \equiv \frac{\partial}{\partial x}, \quad \omega^* \equiv \omega + kV,$$

$$u \equiv v_{x1}, \quad V \equiv v_{y0}.$$

Here,  $\beta_i$  is the ratio of ion pressure to magnetic pressure or ‘‘ion beta.’’

Equation (11) per se is only valid in regions with spatial continuity in  $\rho_0$ ,  $V$ ,  $DV$ , and  $\nu_0$ . For cases involving a discontinuous change in  $\rho_0$ ,  $DV$ , and/or  $\nu_0$  at given values of  $x = x_i$ , Eq. (11) may, however, be integrated across the boundary to obtain jump conditions to match solutions on each side. We assume continuity in  $V$  since we are interested in perturbations with wavelengths on the order of or shorter than the flow sheared layer thickness. Our jump conditions, then, are

$$\Delta_i \left[ (\rho_0 \omega^{*2} - 2k\nu_0 \omega^* D\rho_0) D \left( \frac{u}{\omega^*} \right) + 2k\rho_0(k^2\nu_0 u - (D\nu_0)Du - (i\nu_1)D\omega^*) \right] = \left( \frac{k^2 g u}{\omega^*} \right)_i \Delta_i[\rho_0], \tag{14}$$

$$\Delta_i[V] = 0, \quad \Delta_i[u] = 0. \tag{15}$$

Here,

$$\Delta_i[f(x)] \equiv \lim_{\epsilon \rightarrow 0} (f(x_i + \epsilon) - f(x_i - \epsilon)). \tag{16}$$

Elsewhere, subscript  $i$  refers to the value of a function at  $x = x_i$ , which must be continuous to be well defined (hence  $\Delta_i[u] = 0$  is assumed).

Within any continuous range of  $x$  with uniform  $\rho_0$ ,  $\nu_0$ , and shear factor  $s = DV$  (a positive or negative constant), Eq. (11) reduces to

$$(1 + S)\omega^* D^2 u - (1 - S)\omega^* k^2 u = 2Sk\nu_0 D[D^2 u - k^2 u], \tag{17}$$

$$S = \frac{\beta_i m_i s}{4ZeB_0}.$$

This requires a numerical solution. However, if we confine ourselves to  $|S| \ll 1$  [ $i\nu_1 \approx 0$  from Eq. (12)], Eqs. (17) reduce to the following with the given solution:

$$D^2 u - k^2 u = 0, \quad |S| \ll 1, \tag{18}$$

$$u = \text{constant} \times \exp(i\omega t +iky \pm kx). \tag{19}$$

The effect of both shear and gyroviscosity in this limit, therefore, is due entirely to interaction with neighboring regions via the jump conditions. From Eq. (14), the primary jump condition between two regions with different uniform values of  $\rho_0$ ,  $\nu_0$ , and  $s$  in this limit is

$$\Delta_i \left[ \frac{\rho_0}{\omega^*} (\omega^{*2} Du + (2k^2 \nu_0 \omega^* - s\omega^* - kg)ku) \right] = 0. \tag{20}$$

### III. CASE I: TWO SEMI-INFINITE REGIONS WITH DIFFERENT UNIFORM $\rho_0$ , $s$ , AND $\nu_0$

Here, we define two homogeneous semi-infinite regions separated by a boundary at  $x = 0$  with the following equilibrium properties,

$$\rho_0 = \rho_1, \quad V = s_1 x, \quad \nu_0 = \nu_1 \quad \text{if } x < 0, \tag{21}$$

$$\rho_0 = \rho_2, \quad V = s_2 x, \quad \nu_0 = \nu_2 \quad \text{if } x \geq 0,$$

where  $\rho_1$ ,  $\rho_2$ ,  $s_1$ ,  $s_2$ ,  $\nu_1$ , and  $\nu_2$  are constants (subscript 1 now refers to region 1). Equations (15) and Eq. (19) imply

$$u = \begin{cases} A \exp(kx) & \text{if } x < 0, \\ A \exp(-kx) & \text{if } x \geq 0. \end{cases} \tag{22}$$

Here,  $A$  is an arbitrary constant times  $\exp(i\omega t + ikx)$ , and we confine ourselves to solutions bound for  $x \rightarrow \pm \infty$ . From Eq. (20),

$$\omega^2 - (2k^2 \nu^* - s^*)\omega + kg^* = 0, \tag{23}$$

$$\nu^* = \left( \frac{\nu_2 \rho_2 - \nu_1 \rho_1}{\rho_1 + \rho_2} \right), \quad s^* = \left( \frac{s_2 \rho_2 - s_1 \rho_1}{\rho_1 + \rho_2} \right), \tag{24}$$

$$g^* = g \left( \frac{\rho_2 - \rho_1}{\rho_1 + \rho_2} \right),$$

$$\omega = \left( \nu^* k^2 - \frac{s^*}{2} \right) \pm \sqrt{\left( \nu^* k^2 - \frac{s^*}{2} \right)^2 - g^* k}. \tag{25}$$

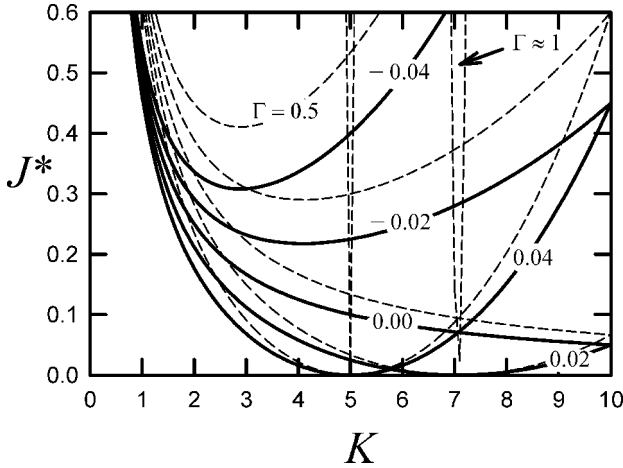


FIG. 1. Case I stability boundary (solid) and associated  $\Gamma=0.5$  and  $0.9999$  contours (dashed, near, and above associated stability boundary) for  $G^* = -0.04, -0.02, 0, 0.02,$  and  $0.04$  (labeled). Rayleigh–Taylor/Kelvin–Helmoltz modes are stable below the respective curves. Note that for  $G^* > 0$ , the stabilizing effect of flow shear is negated (i.e.,  $\Gamma \approx 1$ ) for  $K \approx 1/\sqrt{G^*}$ .

The condition for instability, implying growth rate  $\gamma = \max(-\text{Im } \omega)$ , is

$$J^* > \frac{(1 - G^* K^2)^2}{2K} \rightarrow \Gamma = \sqrt{1 - \frac{(1 - G^* K^2)^2}{2J^* K}}, \quad (26)$$

$$J^* \equiv \frac{g^*}{s^{*2} d}, \quad K \equiv 2kd, \quad G^* \equiv \frac{\nu^*}{2s^* d^2}, \quad \Gamma \equiv \frac{\gamma}{\sqrt{g^* k}}. \quad (27)$$

We reintroduce here  $d$ , the half-thickness of the plasma layer intended to be modeled, for comparison with the normalized representations of case II. The normalization of  $\Gamma$  is chosen so that  $\Gamma = 1$  corresponds to the semi-infinite plasma R–T growth rate in the absence of gyroviscosity and sheared flow.

A clarification of sign conventions is appropriate at this point.  $\nu, g, k$ , and, of course,  $\rho_1$  and  $\rho_2$  are all assumed to be nonnegative. A R–T relevant configuration is one for which  $\rho_2 > \rho_1$ , and may be identified by a positive  $J^*$ .  $G^*$  may be of either sign regardless of the relative magnitudes of  $\rho_1$  and  $\rho_2$ , and takes on the sign of  $s^*$  for  $\nu_2 \rho_2 > \nu_1 \rho_1$ , as is generally the case for R–T configurations. Equation (26) implies configurations with negative  $J^*$  ( $\rho_2 < \rho_1$ ) are always stable. That is, the conventional (statically stable) K–H instability does not occur in case I.

Figure 1 plots the stability boundary and associated  $\Gamma = 0.5$  and  $0.9999$  contours of Eq. (26) for a range of  $G^*$  values. The constant  $\Gamma$  contours are obtained by solving the expression for  $\Gamma$  in Eq. (26) for  $J^*$  and plotting. We see here and from Eq. (26) that there is no global stability (i.e., for all  $K$ ) if  $J^* > 0$  and  $G^* > 0$ , and that gyroviscosity suppresses the stabilizing influence of flow shear in the vicinity of  $K = \sqrt{G^*}$ . We also see that for  $G^* < 0$ , the geometry is stable for all  $K$  if  $J^*$  is sufficiently small. Differentiating the r.h.s. of the inequality in Eq. (26) with reference to  $K$  for a given  $G^* < 0$ , setting equal to zero, and solving for  $K = K_{\text{crit}}$  identifies the (least stable) mode that requires the smallest  $J^*$  to be stable,

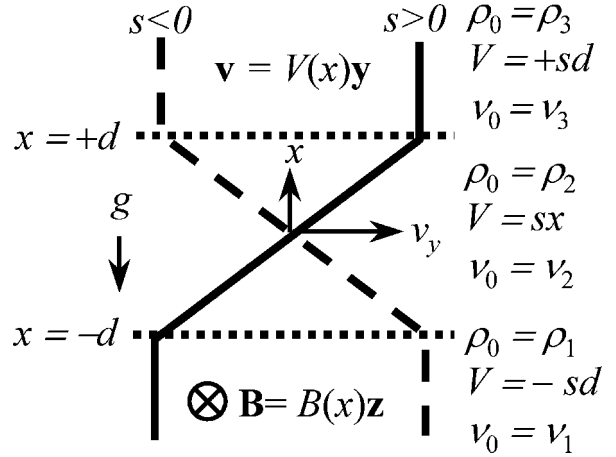


FIG. 2. Geometry and coordinate system assumed for case II—a flow sheared layer separating two unsheared semi-infinite regions. The  $\otimes$  “tail feathers” symbol indicates the magnetic field direction is into the page. The solid/dashed  $V$  vs  $x$  plot corresponds to a positive/negative shear factor  $s$ , given the coordinate conventions.

$$K_{\text{crit}} = \frac{1}{\sqrt{-3G^*}} \quad (G^* < 0). \quad (28)$$

Plugging this back into the inequality gives us our global stability criterion,

$$J^* \leq \begin{cases} 8\sqrt{-G^*/27} & \text{if } G^* < 0 \\ 0 & \text{if } G^* \geq 0. \end{cases} \quad (29)$$

For completeness, we have included the general stability for  $J^* \leq 0$  ( $\rho_2 < \rho_1$ ).

#### IV. CASE II: TWO REGIONS WITH OPPOSING VELOCITIES SEPARATED BY A THIRD REGION WITH A SHEARED TRANSITIONAL VELOCITY PROFILE

To recover a description of the instability known to occur for small  $K$ , and identify other effects of an additional boundary on stability, we assume now the plasma is divided into three regions of uniform  $\rho_0$  and  $\nu_0$ . For this case, we will restrict flow shear to the intermediate region of thickness  $2d$  and drop the “\*” superscripts used to generalize the results. As illustrated in Fig. 2, we have in equilibrium

$$\begin{aligned} \rho_0 &= \rho_1, \quad V = -sd, \quad \nu_0 = \nu_1 \quad \text{if } x < -d, \\ \rho_0 &= \rho_2, \quad V = sx, \quad \nu_0 = \nu_2 \quad \text{if } -d \leq x < +d, \\ \rho_0 &= \rho_3, \quad V = +sd, \quad \nu_0 = \nu_3 \quad \text{if } x \geq +d, \end{aligned} \quad (30)$$

where  $s$  is constant. Equation (19) implies, for bound solutions,

$$\begin{aligned} u &= A_1 e^{+kx} \quad \text{if } x < -d, \\ u &= A_2 e^{+kx} + B_2 e^{-kx} \quad \text{if } -d \leq x < +d, \\ u &= A_3 e^{-kx} \quad \text{if } x \geq +d. \end{aligned} \quad (31)$$

Equations (15) imply

$$\begin{aligned} A_1 e^{-kd} &= A_2 e^{-kd} + B_2 e^{+kd}, \\ A_3 e^{-kd} &= A_2 e^{+kd} + B_2 e^{-kd}. \end{aligned} \quad (32)$$

Substituting Eqs. (30) and Eqs. (31) into Eq. (20), and using Eqs. (32) to eliminate  $A_1$  and  $A_3$ , the primary jump condition may be solved for  $A_2/B_2$  at both boundaries. Equating then gives

$$\frac{(1-\epsilon_3)(1+\Omega_+^2)-2K(G_2-\epsilon_3G_3)\Omega_0\Omega_++2\Omega_0\Omega_+/K}{(1-\epsilon_3)-(1+\epsilon_3)\Omega_+^2-2K(G_2-\epsilon_3G_3)\Omega_0\Omega_++2\Omega_0\Omega_+/K}e^{-2K} = \frac{(1-\epsilon_1)+(1+\epsilon_1)\Omega_-^2-2K(G_2-\epsilon_1G_1)\Omega_0\Omega_-+2\Omega_0\Omega_-/K}{(1-\epsilon_1)(1-\Omega_-^2)-2K(G_2-\epsilon_1G_1)\Omega_0\Omega_-+2\Omega_0\Omega_-/K}, \quad (33)$$

$$\Omega \equiv \frac{\omega}{\sqrt{gk}}, \quad \Omega_0 \equiv \sqrt{\frac{K}{2J}}, \quad \Omega_{\pm} \equiv \Omega \pm \Omega_0, \quad (34)$$

$$K \equiv 2kd, \quad J \equiv \frac{g}{s^2d}, \quad G_i \equiv \frac{\nu_i}{2sd^2}, \quad \epsilon_i \equiv \frac{\rho_i}{\rho_2}.$$

Equation (33) expands into a quartic polynomial in  $\Omega$  with four complex roots. An excellent presentation of the analytic solution to the roots of a quartic polynomial is available.<sup>13</sup> However, the complexity of the final form offers little in the way of physical insight into the stability boundaries, or the ability to formulate simple analytic stability criteria, as was done for case I. Given the availability of math packages that provide complex polynomial roots numerically, that method was chosen instead.

A magnetized plasma layer accelerated by a vacuum field is represented by  $\epsilon_1 = \epsilon_3 = 0$ . Using Laguerre's method<sup>14</sup> for determining the  $\Omega$  solutions, Fig. 3 plots the stability boundaries and several maximum growth rate [ $\Gamma = \max(-\text{Im}\Omega)$ ] contours for  $\epsilon_1 = \epsilon_3 = 0$  and  $G_2 = -0.01$ .  $G_1$  and  $G_3$  have no effect here since  $G_i$  drops out of Eq. (33) if  $\epsilon_i = 0$ . Figure 4, also for  $\epsilon_1 = \epsilon_3 = 0$ , plots stability boundaries for the same values of  $G_2$  as  $G^*$  in Fig. 1 (case I) for comparison. Only the  $\Gamma = 1$  contours are illustrated here to avoid congestion.

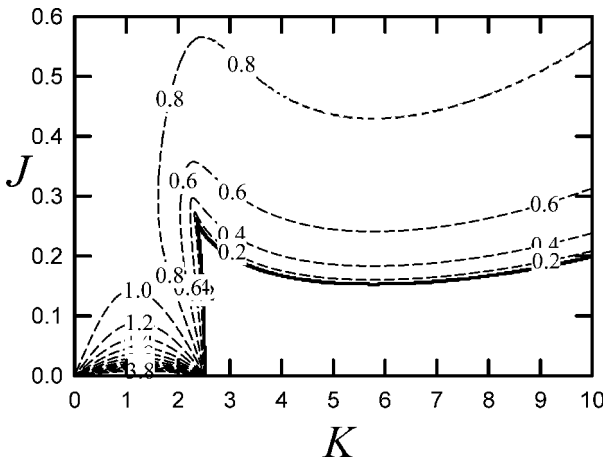


FIG. 3. Stability boundary (solid) and several constant  $\Gamma$  labeled contours (dashed) for case II with  $G_2 = -0.01$  and  $\epsilon_1 = \epsilon_3 = 0$ , representing a magnetized plasma layer accelerated by a magnetic field. Giving the sheared layer a finite thickness results in an unstable low  $K$  region. Note that lowering  $J$  more than necessary to stabilize the high  $K$  region increases  $\Gamma$  in the low  $K$  region.

Figure 5, with  $\epsilon_1 = 0$ , and  $\epsilon_3 = 2$ , represents a flow sheared transitional layer of a magnetically accelerated plasma with a gradual rise in density from vacuum to bulk due to magnetic diffusion. There is a problem, however, in assuming that region 3 represents the unmagnetized bulk since, from Eqs. (3),  $\nu_0 \rightarrow \infty$  as  $B_0 \rightarrow 0$ , causing FLR MHD theory to break down. We assume, therefore, that a semi-infinite *fourth* region some distance (not necessarily  $2d$ ) above region 3 with density  $\rho_4 = 3\rho_2$  represents the unmagnetized bulk. This is only a construction to determine a reasonable value for  $G_3$ ; we will not actually incorporate the new boundary conditions into our model. The flow sheared layer (still confined to region 2), therefore, only penetrates up to the point where the density is  $2/3$  that of the bulk. Since region 4 is assumed very thick compared to the diffusion layer, Eq. (5) implies  $p_0^* = \text{constant}$  may be assumed everywhere of interest. We have, then, from Eqs. (3) and Eqs. (34),  $G_1 = \sqrt{2/3}G_2$  (for reference) and  $G_3 = \sqrt{2}G_2$ . Given this  $G_3$ , the same range of  $G_2$  values used for Fig. 4 are represented in Fig. 5.

## V. PLASMA FOCUS APPLICATION

We now consider the implications of the above to a PF. A PF consists of pair of truncated coaxial electrodes with gas or plasma initially filling the region. Voltage applied across the electrodes creates a current sheath in the intervening medium

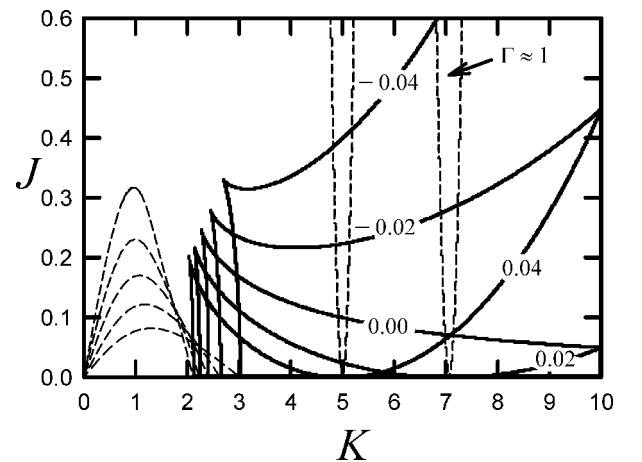


FIG. 4. Stability boundaries (solid) and  $\Gamma \approx 1$  contours (dashed) for case II with  $\epsilon_1 = \epsilon_3 = 0$ , and the same values of  $G_2$  as  $G^*$  in Fig. 1 (case I). Each  $\Gamma = 1$  contour in the low  $K$  region may be matched with its corresponding stability boundary by noticing that they touch at  $J = 0$ . Note the close agreement with Fig. 1 for the high  $K$  region.

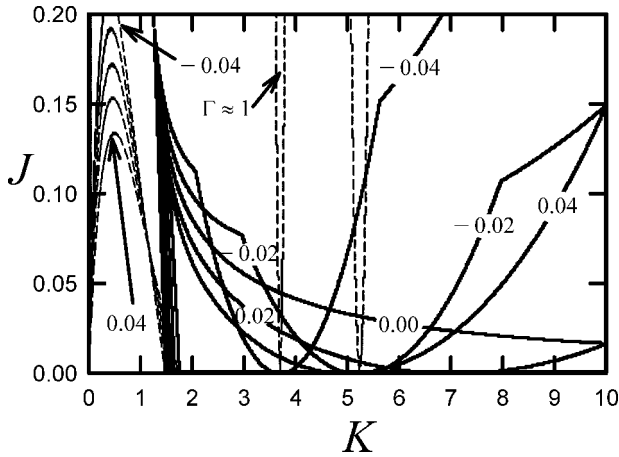


FIG. 5. Stability boundaries (solid) and  $\Gamma \approx 1$  contours (dashed) for case II with  $\epsilon_1=0$ ,  $\epsilon_3=2$ , and the same values of  $G_2$  as  $G^*$  in Fig. 1 (case I).  $G_3=\sqrt{2}G_2$  is assumed. This is intended to represent flow shear within the magnetic diffusion layer of a magnetically accelerated plasma with the continuous rise in density from vacuum to bulk represented by discrete steps. The degraded high  $K$  stability relative to Fig. 4 is traceable to the addition of a second (upper) unstable interface with opposite  $G^*$  when analyzed in terms of the case I model (see Sec. VI).

which forms a magnetic pressure driven mass accreting shocked layer that propagates primarily in the axial direction until the end of the inner electrode is reached. Thereafter, the inner part of the shocked layer bends radially inward, implodes, and forms a Z pinch on axis. Barring significant mixing across the shocked layer, the axial momentum of plasma accreted during the earlier phase is retained during the implosion phase, while plasma accreted during the implosion has less axial momentum. The resultant characteristic flow shear factor may be expressed as

$$s = \pm \eta V_0 / 2d, \tag{35}$$

where  $V_0$  is the speed of the current sheath and, in anticipation of the application of case II,  $2d$  is the shocked layer thickness.  $\eta$  is the efficiency by which the shocked layer is sheared, with an optimally designed system having a value close to unity by the time of the final pinch.

Figure 6 illustrates the geometry of case II (Fig. 2) applied to the PF accretion phase. It is not to scale, and the shape of the electrodes is chosen simply to make the figure as compact as possible, as opposed to suggesting a preferred profile. The axes and dashed line represent the coordinate system and negative  $s$  velocity curve of Fig. 2, respectively. The origin is assumed to be tied to the accelerated reference frame of a fluid element at intermediate depth within the accretion layer. The geometry has been rotated about the  $z$ -axis to align the  $x$  direction with that of acceleration, and then rotated about the  $x$ -axis by  $180^\circ$  so that the magnetic field is pointing out of the paper, as represented by the  $\odot$  “arrow point” symbol. The  $s < 0$  profile and the latter rotation are necessary to represent the sheared velocity profile of a PF with a central anode. Without the latter rotation, the  $s > 0$  (solid) curve of Fig. 2 would represent the velocity profile resulting from PF dynamics, and the magnetic field would be pointing into the paper, as in the original figure. This would make the center conductor the cathode.

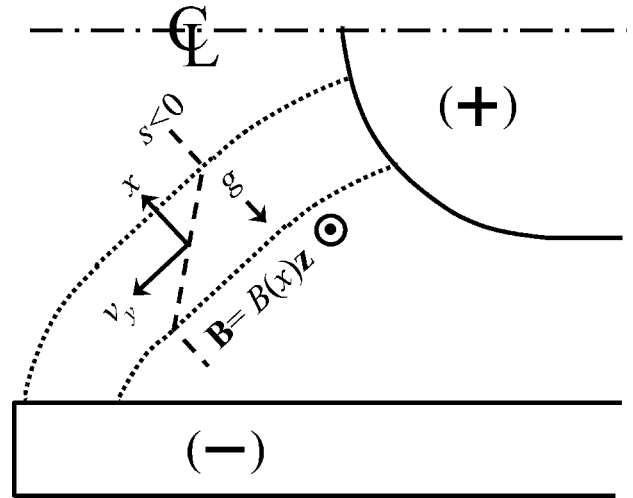


FIG. 6. Application of case II geometry (Fig. 2) with  $\epsilon_1=\epsilon_3=0$  to the plasma focus accretion phase. Only the negative  $s$  velocity curve of Fig. 2 is represented so as to corresponded a plasma focus with a central anode. The origin is assumed to be tied to the accelerated reference frame of a fluid element at mid-depth within the accretion layer. In addition to the geometry being rotated about the  $z$ -axis to align the  $x$  direction with that of acceleration, it is rotated about the  $x$ -axis by  $180^\circ$  so that the magnetic field is now pointing out of the paper (as represented by the  $\odot$  “arrow point” symbol).

We may make an estimate of effective case II model parameters based on PF system parameters via the planar “snow plow” model<sup>15,16</sup> of plasma accretion used in conjunction with a more detailed planar model<sup>17</sup> that provides self-similar solutions to the accretion layer’s density profile. The former assumes that the layer is thin enough to neglect its internal structure for the purposes of overall momentum and mass conservation. For our purposes this means

$$\frac{B_0^2}{2\mu_0} = \frac{d}{dt}(\sigma V_0), \quad \sigma = \rho_f L, \quad V_0 = \frac{dL}{dt}, \tag{36}$$

where  $\sigma$  is the layer’s mass per unit area,  $\rho_f$  is an assumed uniform initial gas fill density,  $L=L(t)$  is the distance propagated by the current sheath, and  $B_0$  is the magnetic field magnitude driving the layer. The more detailed model applies to cases where a thin current sheath propagates through an initially cold uniform gas according to the power law

$$L = a \frac{t^n}{n}, \quad n \geq 1 \tag{37}$$

or, alternately, the exponential law

$$L = g_0 t_0^2 \exp\left(\frac{t}{t_0}\right). \tag{38}$$

The density profile near the current sheath for the power law is approximately

$$\rho = \rho_f N_1 \left(\frac{x}{L}\right)^{-\alpha}, \quad \alpha = \frac{2(n-1)}{n(\gamma+2)-2}, \tag{39}$$

where  $x$  here is distance ahead of the sheath,  $\gamma$  is the specific heats ratio, and  $N_1=N_1(n, \gamma)$  is determined numerically. This model implies a current sheath pressure only slightly larger than the thin layer limit of Eqs. (36), at least for  $n$

≥1.5, and is appropriate if radiation may be neglected, which can result in the collapse of the layer thickness.<sup>18</sup>

To determine case II model parameter  $J$ , a reasonable choice for  $d$  is the distance in front of the sheath that  $\rho$  must be integrated to equal  $\sigma/2$ . From Eqs. (36), Eq. (37), and Eqs. (39), the result is

$$d = L \left( \frac{1-\alpha}{2N_1} \right)^{1/(1-\alpha)} = a \frac{t^n}{n} \left( \frac{1-\alpha}{2N_1} \right)^{1/(1-\alpha)}. \quad (40)$$

Noting from Eq. (37) that

$$V_0 = \frac{dL}{dt} = at^{n-1}, \quad g = \frac{d^2L}{dt^2} = (n-1)at^{n-2}, \quad (41)$$

Eqs. (34), Eq. (35), and Eq. (40) give us

$$J = \frac{4gd}{\eta^2 V_0^2} = \frac{4(n-1)}{n\eta^2} \left( \frac{1-\alpha}{2N_1} \right)^{1/(1-\alpha)}. \quad (42)$$

To estimate  $G_2$ , we take the magnetic pressure  $B_0^2/2\mu_0$  driving the layer, and  $\rho_2 = \sigma/(2d)$  to be the characteristic plasma pressure and density, respectively. The characteristic  $T$  may then be determined from the ideal gas law

$$\frac{B_0^2}{2\mu_0} = \frac{\sigma}{2m_i d} k_B T. \quad (43)$$

Using Eq. (37) in Eqs. (36), meanwhile, gives

$$\frac{B_0^2}{2\mu_0} = \frac{(2n-1)}{n} \rho_f a^2 t^{2n-2}. \quad (44)$$

Equating this to Eq. (43), and using Eqs. (36) and Eq. (40), we solve for

$$k_B T = 2(2n-1)m_i a^2 \left( \frac{t^{2n-2}}{n} \right) \left( \frac{1-\alpha}{2N_1} \right)^{1/(1-\alpha)}. \quad (45)$$

We now assume  $T_i = T_e = T/(1+Z)$ . This allows us to use Eq. (44) solved for  $B_0$  and Eq. (45) in Eqs. (3) to obtain

$$v_2 = \frac{m_i a t^{n-1} \sqrt{2n-1}}{eZ(1+Z)\sqrt{2n\mu_0\rho_f}} \left( \frac{1-\alpha}{2N_1} \right)^{1/(1-\alpha)}. \quad (46)$$

This implicitly assumes a total plasma beta  $\beta \equiv (\rho_2 k_B T/m_i)/(B_0^2/2\mu_0) \sim 1$ . Substituting this, Eq. (35) [using Eqs. (41)], and Eq. (40) into Eqs. (34) gives

$$G_2 = \pm \frac{v_2}{\eta V_0 d} = \pm \frac{m_i \sqrt{2n-1}}{eZ(1+Z)\eta L \sqrt{2n\mu_0\rho_f}}, \quad (47)$$

where  $\pm = +$  or  $-$  for a central cathode or anode, respectively.

In general, we find that  $J$ , as determined by Eq. (42), is small enough for the large  $K$  stability criterion for a PF with a central anode to be represented by case I Eq. (29) with  $G^* = G_2$ , or

$$|G_2| > 27 \left( \frac{J}{8} \right)^2 \quad (G_2 < 0). \quad (48)$$

From this, Eq. (42), Eq. (47), Eq. (37) and Eq. (44) solved for  $\rho_f$ , our stability criterion may be written as

$$\frac{eZ(1+Z)B_0 t}{\eta^3 m_i} = \frac{eZ(1+Z)L}{\eta^3 m_i} \sqrt{2\mu_0 n(2n-1)\rho_f} < \frac{4n^2(2n-1)}{27(n-1)^2} \left( \frac{2N_1}{1-\alpha} \right)^{2/(1-\alpha)}. \quad (49)$$

Equation (28), Eq. (48), and Eq. (42), meanwhile, imply that the first wave number to go unstable as  $B_0 t$  is raised beyond the stability threshold is

$$K_{\text{crit}} = \frac{8}{9J} = \frac{2n\eta^2}{9(n-1)} \left( \frac{2N_1}{1-\alpha} \right)^{1/(1-\alpha)}. \quad (50)$$

A case of special interest is  $\gamma = 5/3$  (monatomic ideal gas) and  $n = 2$  [ $\alpha = 3/8$ , from Eqs. (39)]. From Eq. (44), this  $n$  corresponds to the initial linearly rising  $B_0$  of a capacitatively driven inductive load typical of most PF circuits. From Eqs. (41), it also means  $g = a$  (constant). The value of  $N_1$  in this case may be inferred from the numerical solutions plotted in Gol'berg and Velikovich<sup>17</sup> Fig. 4 and G-V Eq. (A6). To this end, let  $x_s$  be the distance in front of the current sheath of the shock front that precedes it ( $\eta_s = x_s/L$  in G-V's notation). G-V Fig. 4 ( $N$  plot) shows  $\rho = 11.5\rho_f$  at  $x = 0.1x_s$ , while  $x_s = 0.16L$  based on G-V Fig. 4 ( $-U$  plot) and G-V Eq. (A6). Equations (39), Eq. (42), Eq. (48), and Eq. (50) then imply, for a high  $K$  stable PF with a central anode,

$$n = 2, \quad \gamma = 5/3, \quad \alpha = 3/8, \quad N_1 = 2.44, \quad (51)$$

$$J = \frac{0.0746}{\eta^2}, \quad |G_2| > \frac{2.35 \times 10^{-3}}{\eta^4}, \quad K_{\text{crit}} = 11.9 \eta^2.$$

From Eq. (49), the stability criterion may be written,

$$\frac{eZ(1+Z)B_0 t}{\eta^3 m_i} = \frac{2eZ(1+Z)L}{\eta^3 m_i} \sqrt{3\mu_0\rho_f} < 1277. \quad (52)$$

As a check on the accuracy of our  $\rho$  approximation [Eqs. (39)],  $N_1$  inferred for the above case, Eq. (40), and Eqs. (39) imply  $\rho = 8.37\rho_f$  at  $x = d = 0.0373L$ . G-V Fig. 4, meanwhile, shows  $\rho = 8.2\rho_f$  at  $x/x_s = d/x_s = 0.233$  ( $\eta/\eta_s$  in their notation). These similar values for  $\rho$  retroactively validates the use of Eq. (39) (valid for  $x \ll x_s$ ) for the purposes of integration out to  $x = d$ .

The case where  $L$  increases exponentially [Eq. (38)] results in the same density profile plotted by G-V Fig. 4 and approximated by Eqs. (39) for  $x \ll x_s$  in the limit  $n \rightarrow \infty$ .<sup>17</sup> This is another case of special interest since it results from the exponential current waveform characteristic of a magnetic flux compression generator.<sup>19</sup> The expression for  $d$  in terms of  $L$  in Eq. (40) is still valid. However, Eqs. (41) are replaced by

$$V_0 = \frac{L}{t_0} = g_0 t_0 \exp\left(\frac{t}{t_0}\right), \quad g = \frac{L}{t_0^2} = g_0 \exp\left(\frac{t}{t_0}\right). \quad (53)$$

Equations (34), Eq. (35), Eq. (38), and Eq. (40) then result in

$$J = \frac{4}{\eta^2} \left( \frac{1-\alpha}{2N_1} \right)^{1/(1-\alpha)}. \quad (54)$$

Equation (43) may still be used to determine  $k_B T$  for use in calculating  $G_2$ , but it is now equated to, from Eqs. (36), Eq. (38), and Eqs. (53),

$$\frac{B_0^2}{2\mu_0} = 2\rho_f g_0^2 t_0^2 \exp\left(\frac{2t}{t_0}\right). \quad (55)$$

Proceeding as before with the help of Eqs. (36), Eq. (40), Eqs. (3), Eqs. (34), Eq. (35), Eqs. (53), and Eq. (55) solved for  $B_0$ ,

$$k_B T = 4m_i g_0^2 t_0^2 \exp\left(\frac{2t}{t_0}\right) \left(\frac{1-\alpha}{2N_1}\right)^{1/(1-\alpha)}, \quad (56)$$

$$v_2 = \frac{m_i g_0 t_0}{Z(1+Z)e\sqrt{\mu_0\rho_f}} \exp\left(\frac{t}{t_0}\right) \left(\frac{1-\alpha}{2N_1}\right)^{1/(1-\alpha)}, \quad (57)$$

$$G_2 = \pm \frac{v_2}{\eta V_0 d} = \pm \frac{m_i}{eZ(1+Z)\eta L\sqrt{\mu_0\rho_f}}. \quad (58)$$

Not surprisingly, the normalized forms of Eq. (54) and Eq. (58) correspond to  $n \rightarrow \infty$  of Eq. (42) and Eq. (47), respectively. G–V Eq. (A6) still follows from the Hugoniot relations, so the same procedure as before may be used to determine  $N_1$ . Specifying now for an ideal gas, Eqs. (39), Eq. (54), Eq. (48), and Eq. (50) imply, for a high  $K$  stable PF with a central anode,

$$\begin{aligned} \gamma &= 5/3, \quad \alpha = 6/11, \quad N_1 = 1.467, \\ J &= \frac{0.0661}{\eta^2}, \quad |G_2| > \frac{1.843 \times 10^{-3}}{\eta^4}, \quad K_{\text{crit}} = 13.4\eta^2. \end{aligned} \quad (59)$$

From Eq. (58), Eq. (38), and Eq. (55) solved for  $\rho_f$ , our stability criterion is

$$\frac{eZ(1+Z)B_0 t_0}{\eta^3 m_i} = \frac{eZ(1+Z)L}{\eta^3 m_i} \sqrt{2\mu_0\rho_f} < 767. \quad (60)$$

The values of  $B_0$  and  $L$  in terms of machine parameters are still vague at this point. A conservative choice for  $B_0$  would be  $B$  at the radius  $R_1$  of the center conductor given machine current  $I$  and Ampère's law. Meanwhile, optimizing  $\eta$  entails balancing the mass accreted during the axial acceleration phase with that of the radial implosion phase. This suggests that the inner electrode length should be comparable to its radius. Specifying henceforth our dynamic parameters to be their values at pinch time, we therefore assume

$$B_0 = \frac{\mu_0 I}{2\pi R_1}, \quad L = 2R_1. \quad (61)$$

Given this, an interesting result is obtained by constraining the various cases' stability criteria with the following empirical scaling constant for  $D_2$  PF optimized for maximum neutron yield,<sup>20</sup>

$$C = \frac{I}{R_1 \sqrt{\rho_f}} = 5.79 \times 10^8 \left( \frac{\text{A}\cdot\text{m}^{1/2}}{\text{kg}^{1/2}} \right). \quad (62)$$

From Eqs. (61), Eq. (49), Eq. (52), and Eq. (60), then,  $R_1$  and the high  $K$  stability criterion for an optimal  $D_2$  PF ( $Z$

= 1) for arbitrary  $n$ , a linearly ramped current ( $n=2$ ), and an exponentially rising current are, respectively,

$$\begin{aligned} R_1 &= \frac{\sqrt{\mu_0} C t}{4\pi\sqrt{2n(2n-1)}} \quad (\text{power law}), \\ I/\eta^3 &< \frac{n\sqrt{2n(2n-1)}}{27(n-1)^2} \left( \frac{2N_1}{1-\alpha} \right)^{2/(1-\alpha)} \frac{C m_i}{eZ(1+Z)\sqrt{\mu_0}}, \end{aligned} \quad (63)$$

$$\begin{aligned} R_1 &= \frac{\sqrt{\mu_0} C t}{8\pi\sqrt{3}} = 1.49 \times 10^4 t \quad \text{m/s (linear)}, \\ I/\eta^3 &< 184.3 \frac{m_i C}{eZ(1+Z)\sqrt{\mu_0}} = 2.0 \quad \text{MA}, \end{aligned} \quad (64)$$

$$\begin{aligned} R_1 &= \frac{\sqrt{\mu_0} C t_0}{4\pi\sqrt{2}} = 3.65 \times 10^4 t_0 \quad \text{m/s (exp)}, \\ I/\eta^3 &< 271.2 \frac{C m_i}{eZ(1+Z)\sqrt{\mu_0}} = 2.9 \quad \text{MA}. \end{aligned} \quad (65)$$

We are reminded that the perturbation profile used to derive the above stability criteria assumes  $|S| \ll 1$  [Eq. (18)]. We assumed  $\beta = 1$ , making  $\beta_i = 1/(1+Z) = 1/2$  so, from Eqs. (17), Eq. (35), Eq. (40), and Eqs. (41),

$$|S| = \frac{n}{8\eta^2} \left( \frac{\eta^3 m_i}{eZ(1+Z)B_0 t} \right) \left( \frac{2N_1}{1-\alpha} \right)^{1/(1-\alpha)} \quad (66)$$

for the power law current. The term in the first parenthesis is the inverse of the l.h.s. of Eq. (49), or Eq. (52) for  $\gamma = 5/3$  and  $n=2$ . From Eqs. (51), then, we have  $|S| = 5.2 \times 10^{-3}/\eta^2$  for an ideal gas driven by a linear current ramp at the stability threshold. A similar analysis using Eq. (35), Eq. (40), Eqs. (53), Eqs. (59), and Eq. (60) shows  $|S| = 9.9 \times 10^{-3}/\eta^2$  at the stability threshold of an exponential current driving an ideal gas. The stability criteria, therefore, may be considered valid for  $\eta \sim 1$  during most of the discharge for systems approaching critical parameters. At very early times or for much less energetic systems, however, we can have  $|S| \sim 1$  due to a smaller  $B_0 t$ . Having not been solved, the stability implications of the numerical solution to Eqs. (17) in such cases are unclear.

## VI. DISCUSSION

Comparison of Fig. 1 to Fig. 4 indicates that for  $0 < J \leq 0.3$  and  $G_2 \leq 0$ , Eq. (29) with  $G^* = G_2$  suffices as the large  $K$  stability criterion for an accelerated layer ( $\epsilon_1 = 0$ ,  $\epsilon_3 = 0$ ), as used in Sec. V. Note in Fig. 5, though, that for  $G_2 = 0$ , the critical  $J$  for a given  $K$  is 3 times lower than in the corresponding curve of Fig. 4. This is traceable to the additional unstable upper boundary due to  $\epsilon_3 = 2$  in the former. Specifically, application of the case I semi-infinite model to this boundary (appropriate for large  $K$ ) shows that, from Eqs. (24),  $s^* = -s_1/3$  there, where  $s_1$  in this context is the shear factor  $s$  of the transitional layer, and  $g^* = g/3$ . From Eqs. (27),  $J^*$  is, therefore, amplified relative to  $J$  in case II [as defined in Eqs. (34)] by a factor of 3. Worse still, due to the

above  $s^*$  sign reversal,  $G_2 < 0$  in Fig. 5 (favorable for the lower boundary) implies an unfavorable  $G^* > 0$  for the upper boundary. This explains the unstable wave number that occurs for all  $J$  for both. This indicates that, if gyroviscosity effects are to be exploited or otherwise significant, flow shear should extend further than the density transition layer of the current sheath. Attempts to confine the sheared flow to the diffuse layer where the density rises within the magnetic skin depth, as has been suggested,<sup>4</sup> are likely to be counterproductive.

The validity of the stability criteria derived here depend on the ability to treat instabilities, especially the least stable mode with  $K = K_{\text{crit}}$  ( $k = k_{\text{crit}}$ ), in terms of incompressible motion. Relevant references involving compressible media were sought for insight. In the absence of flow shear, R–T modes resulting from a discontinuity in an ideal compressible fluid have the same growth rate for wavelengths short relative to the vertical scale length, and compressibility reduces the growth rate for longer wavelengths.<sup>21</sup> Our high  $K$  stability criteria, therefore, should not be affected on this account. As for flow shear effects, however, it is clear from a compressible ideal MHD analysis corresponding to our case II geometry with  $\epsilon_3 = \epsilon_1 = 1$  and  $g = 0$ ,<sup>22</sup> that our incompressibility assumption requires the magnetoacoustic mach number, defined as the ratio of the characteristic shear speed to the magnetoacoustic speed  $c_m$ , to be much less than unity. In general, the characteristic shear speed for case II is  $|s|d$ . If, however, we are primarily concerned with whether or not a particular wave number  $k \gg 1/d$  behaves in an incompressible manner, the *mode's* characteristic speed is  $|s|/k$ . The general and high wave number ratios are, then, respectively,

$$M = \frac{|s|d}{c_m}, \quad M_k = \frac{|s|}{kc_m}, \quad c_m = \sqrt{\frac{B_0^2(\gamma\beta + 2)}{2\mu_0\rho_2}}. \quad (67)$$

For a PF with power law current, from  $\beta = 1$ , Eqs. (27), Eq. (35), Eqs. (41), Eq. (43) ( $\rho_2 = \sigma/(2d)$ ), and Eq. (45),

$$M = \frac{\eta\sqrt{n}}{\sqrt{8(2n-1)(\gamma+2)}} \left( \frac{2N_1}{1-\alpha} \right)^{1/(2-2\alpha)}, \quad M_K = \frac{2M}{K}. \quad (68)$$

For an ideal gas driven with a linear current rise,  $M$  and  $M_K$  for  $K = K_{\text{crit}}$  are, from Eqs. (51),  $M = 0.78\eta$  and  $M_{\text{crit}} = 0.13/\eta$ , respectively. Meanwhile, for an ideal gas driven with an exponential current rise, from Eqs. (53), Eq. (43), Eq. (56), and Eqs. (59),  $M = 1.01\eta$  and  $M_{\text{crit}} = 0.151/\eta$ . So for  $\eta \sim 1$ , our incompressible model is marginally suitable at best for low  $K$ , but adequate for the purposes of our PF high  $K$  stability criteria [Eqs. (63), Eqs. (64), and Eqs. (65)].

Another complication due to compressibility is the effect on  $B$  due to the Hall term added to generalized Ohm's law in nonideal MHD.<sup>23</sup> Since the only occurrences of  $B$  in our governing equations [Eqs. (1)–(4)] are absorbed into the definitions of  $p^*$ , which is eliminated, and  $\nu$ , which is carried through as an independent parameter, and our equation of state  $\nabla \cdot \mathbf{v} = 0$  has no independent plasma pressure dependence, generalized Ohm's law is not needed for mathematical closure. The Hall term can, nonetheless, result in unstable

R–T modes due to actual compressibility. Ideal MHD is generally adequate for describing a given mode provided<sup>23</sup>  $F \equiv kr_i \ll 1$  and  $H \equiv ck/\omega_{pi} \ll 1$ , where

$$r_i = \frac{\sqrt{m_i k_B T_i}}{ZeB_0}, \quad \omega_{pi} = \sqrt{\frac{\rho_0 Z^2 e^2}{\epsilon_0 m_i^2}}, \quad (69)$$

are the Larmor radius and ion plasma frequency, respectively. The FLR stress tensor and Hall terms extend the range to  $F \lesssim 1$  and<sup>24</sup>  $H \gtrsim 1$ , respectively. Since we include the former and neglect the latter,  $F_{\text{crit}} \equiv k_{\text{crit}} r_i \lesssim 1$  and  $H_{\text{crit}} \equiv ck_{\text{crit}}/\omega_{pi} \lesssim 1$  are additional conditions for the validity of our stability criteria. Unlike the conditions on  $M$ , satisfying these conditions at  $k_{\text{crit}}$  automatically satisfies them for smaller  $k$ . For both the power law and exponential currents in our PF example we have, from Eq. (43) ( $T_i = T_e = T/(1+Z)$ ), Eqs. (36), and Eq. (40),

$$F = \frac{Km_i}{2ZeL\sqrt{(1+Z)\mu_0\rho_f}} \left( \frac{2N_1}{1-\alpha} \right)^{1/(2-2\alpha)},$$

$$H = \frac{cKm_i}{ZeL} \sqrt{\frac{\epsilon_0}{2\rho_f}} \left( \frac{2N_1}{1-\alpha} \right)^{1/(2-2\alpha)}. \quad (70)$$

Substituting in Eq. (49) solved for  $L\sqrt{\rho_f}$ , and Eq. (50) for  $K$ , we have for a power law current

$$F_{\text{crit}} = \frac{3(n-1)\sqrt{2(1+Z)}}{4\eta\sqrt{n(2n-1)}} \left( \frac{1-\alpha}{2N_1} \right)^{1/(2-2\alpha)},$$

$$H_{\text{crit}} = \frac{3(n-1)(1+Z)}{2\eta\sqrt{n(2n-1)}} \left( \frac{1-\alpha}{2N_1} \right)^{1/(2-2\alpha)}. \quad (71)$$

For an ideal gas driven by a linear current rise, from Eqs. (51),

$$F_{\text{crit}} = 0.084\sqrt{1+Z}/\eta, \quad H_{\text{crit}} = 0.118(1+Z)/\eta. \quad (72)$$

Meanwhile, for an exponential current rise, from Eqs. (70), Eqs. (59), and Eq. (60),

$$F_{\text{crit}} = 0.096\sqrt{1+Z}/\eta, \quad H_{\text{crit}} = 0.136(1+Z)/\eta. \quad (73)$$

Hence our  $F_{\text{crit}}$  and  $H_{\text{crit}}$  conditions are satisfied for  $\eta \sim 1$ . In fact, these values are so low that, taken at face value, one would expect ideal MHD to be adequate *precisely* at the point where FLR stabilization appears. The reason for the discrepancy is that the  $F_{\text{crit}} \ll 1$  condition for ideal MHD is a general rule, and does not fully account for the enhanced significance of gyroviscosity in a strongly flow sheared plasma that results from the large (zeroth order) coupling in Eqs. (2). There is no analogous amplifying effect on the significance of the Hall term. However, it is possible that compressible Hall modes come into play at much higher values of  $K$  than  $K_{\text{crit}}$ .

Equations (63), Eqs. (64) and Eqs. (65) do not necessarily imply that a neutron optimized D<sub>2</sub> PF operating at greater than the critical current will emit fewer neutrons than one operating at that current. If that were the case, conventional (unstable) Z pinches without sheared flow would not work as they do. A more reasonable prediction is that there will be a diminished return on increasing the current. The  $I^4$  neutron

production scaling law<sup>25</sup> may break down, for example. Furthermore, the presented model involves crude approximations of PF dynamics, so the ultimate current threshold may be significantly different, even if care is taken to make  $\eta$  as close to unity as possible. The calculations presented suggest only that there is such a current threshold in the general vicinity of the estimates. To test the theory empirically does not necessarily require current exceeding the neutron optimized limit. The more general  $B_0 t$  threshold may be studied at lower current by reducing the anode diameter and looking for evidence of instability with wave numbers of the order predicted by Eqs. (50), Eqs. (51), or Eqs. (59), as the case may be, with interferometric, Schlieren, or other types of imaging systems.

$B_0$ ,  $t$ , and/or  $I$  limits for PF stability are relaxed significantly for current drivers with a high effective  $n$  or, ideally, an exponential current rise. From Eq. (60), for example, there is no  $t$  constraint per se to reach the a desired  $B_0$ , as long as the  $e$ -fold time  $t_0$  remains small enough. Furthermore, Eqs. (64) and Eqs. (65) suggest that stable operation of a neutron optimized  $D_2$  PF with currents roughly 50% higher may be possible for an exponential vs linear drive. Note also that if  $m_i C / (Z(1+Z))$  is increased for PF applications such as x-ray production, a proportionately higher current threshold is implied.

The description in Sec. V as to how to employ the geometry of Fig. 2 to a PF (Fig. 6) was decidedly descriptive, making simple use of Ampère’s law and the right hand current rule. A more general local definition of  $s$  in terms of the unperturbed velocity field  $\mathbf{v}_0$  and local unit vectors appropriate for the model is

$$s \equiv \mathbf{x} \cdot \nabla (\mathbf{v}_0 \cdot \mathbf{y}), \quad \mathbf{z} = \mathbf{B} / |\mathbf{B}|, \tag{74}$$

$$\mathbf{x} = - \frac{\partial^2 \mathbf{v}_0}{\partial t^2} \Big/ \left| \frac{\partial^2 \mathbf{v}_0}{\partial t^2} \right|, \quad \mathbf{y} = \mathbf{z} \times \mathbf{x}.$$

Using this form, local definitions of case I parameters may be used to make predictions based on results such as Eq. (26), Eq. (29), and the instability of  $K \approx \sqrt{G^*}$  for  $G^* > 0$ . To this end, Eqs. (27) may be rewritten

$$J^* = \frac{4g\bar{\rho}(\Delta\rho/\Delta x)}{(\Delta(s\rho)/\Delta x)^2 L^2}, \quad G^* = \frac{2\Delta(v\rho)/\Delta x}{L^2\Delta(s\rho)/\Delta x},$$

$$\Gamma = \frac{\gamma\sqrt{2\bar{\rho}}}{\sqrt{gkL\Delta\rho/\Delta x}}, \quad K = kL,$$

$$L \equiv 2d, \quad \bar{\rho} \equiv (\rho_1 + \rho_2)/2, \quad \Delta x \equiv L, \tag{75}$$

elsewhere  $\Delta Q \equiv Q_2 - Q_1$ .

These suggest local definitions

$$J^* \equiv \frac{4g\rho_0 D\rho_0}{(LD(s\rho_0))^2}, \quad G^* \equiv \frac{2D(v_0\rho_0)}{L^2 D(s\rho_0)}, \tag{76}$$

$$\Gamma \equiv \frac{\gamma\sqrt{2\rho_0}}{\sqrt{gkLD\rho_0}}, \quad K \equiv kL.$$

$L$ , here, may then be interpreted as the characteristic equilibrium scale length. These forms may be used to predict

unstable configurations for a wider range of accelerated plasma configurations than the simplified cases presented.

If we assume that  $\nu$  and, therefore  $B$ , are a space–time constants ( $T$  is already assumed so), Eq. (11) reduces to

$$D \left[ \omega^*(\rho_0\omega^* - 2\nu k D\rho_0) D \left( \frac{u}{\omega^*} \right) \right] = k^2 \left( (\rho_0\omega^{*2} + (g - 2k\nu\omega^*)D\rho_0) \left( \frac{u}{\omega^*} \right) \right). \tag{77}$$

This is equivalent to Rosenbluth and Simon’s Eq. (3.12),<sup>26</sup> except that we neglect R–S parameter  $b$  [R–S Eq. (3.7)], and the direction of gravity is reversed. It corresponds to low plasma  $\beta$  (where  $\mathbf{B}$  is dominated by its vacuum solution), referred to in R–S as the “flute approximation.”  $b$  is the ratio of the Alfvén speed to the speed of light and, as in ideal MHD, does not appear as a result of the neglect of the displacement current in Eq. (1). To derive the former from the latter,  $P/\Omega$  (R–S notation)  $= p_i/\omega_{pi} = 2\rho_0\nu$  is used to find an expression for R–S parameter  $T$  (not related to temperature) in terms of our variables, and the equilibrium and first order contributions to R–S Eq. (2.25), with the help of Eq. (9) and Eq. (10), are used to find an expression for R–S parameter  $\psi$ . With  $b=0$ , then,

$$T = \omega^*(\rho_0\omega^* - 2\nu k D\rho_0), \quad \psi = B \frac{u}{\omega^*}. \tag{78}$$

Interestingly, while both Eq. (77) and R–S Eq. (3.12) assume  $B \approx \text{constant}$ , the latter is stated to allow for spatial variations in temperature. Being equivalent, this implies Eq. (77) also allows for such variations, but we have not shown this since Eq. (77) is derived using the isothermal FLR stress tensor.<sup>10</sup> The simplest interpretation is that R–S Eq. (3.12) does not simplify in the isothermal case.

As for connections to other work, Eq. (77) with  $\nu=0$  reduces to Goldstein’s<sup>3</sup> Sec. II, Eq. (11) or, equivalently, to Chandrasekhar’s Chap. 11, Eq. (21).<sup>7</sup> Equation (33) with  $G_i=0$  reduces to Taylor’s<sup>6</sup> Eq. (25). The  $G_2=0$  plots of Fig. 4 and Fig. 5 correspond to Shumlak and Roderick’s<sup>5</sup> Fig. 4 and Ruden’s<sup>4</sup> Fig. 2, respectively. Where  $\nu$  is considered, Eq. (77) reduces to Huba’s<sup>27</sup> Eq. (9) for  $V=0$ , although  $T$  should have been defined as  $T_i$  in the latter. For the case where  $\rho_0$  increases with height as  $\exp(\lambda x)$  and  $V=0$ , solutions to Eq. (77) bound at infinity (requiring  $Du=0$ ) reduce to Roberts and Taylor’s<sup>9</sup> Eq. (7), which results in stability for  $k^2 \geq g/\nu^2\lambda$ . Significantly, Qiu, Huang, and Juan’s<sup>28</sup> Eq. (4), which assumes the kinematic viscosity force density vector  $\nu\rho\nabla^2\mathbf{v}$  may be used to model gyroviscosity, results in

$$\omega^2 - i\nu k^2\omega + g\lambda = 0 \rightarrow \gamma = \sqrt{g\lambda + \frac{k^4\nu^2}{4}} - \frac{k^2\nu}{2} \tag{79}$$

for this case, based on Q–H–J Eq. (21) with its  $\omega$  sign convention reversed to correspond to ours. This solution is unstable for *all*  $k$ , merely damping modes with higher  $k$  (as is typical of kinematic viscosity).

## VII. SUMMARY/CONCLUSIONS

The general dispersion relation for magnetically transverse modes of an isothermal incompressible FLR MHD plasma in a gravitational field with depth dependent density and horizontal flow is derived and used to model the stability of an accelerated plasma layer with sheared flow. To illustrate its utility, the electrode polarity dependence of plasma focus performance is explained as a natural consequence of the coupling of gyroviscosity to the sheared flow inherent in PF dynamics. For a given current waveform and a central anode, an upper bound on the value of  $B_0$  used to drive a PF plasma for a given for current delivery time [scale] for high wave number stability is implied. A minimum anode radius is, therefore, implied for a given current driver. Constraining the stability criteria further with a previously recognized empirical scaling law for a neutron yield optimized  $D_2$  PF [Eq. (62)], an absolute maximum current for stable operation is implied for a given current waveform, independent of rise time.

Like any analytic plasma theory, the results should be interpreted skeptically. Electrical resistivity, turbulent mixing, compressible Hall modes, and the more complex actual current sheath trajectory of a PF could all have a significant impact on the accuracy of predictions. At a very minimum, the results are intended to demonstrate that the coupling of gyroviscosity to sheared flow may be significant in some plasma devices for which FLR effects have generally been ignored. The stability characteristics of the equilibrium pinched state of shear flow stabilized Z pinch,<sup>29</sup> for example, may be affected.

- <sup>1</sup>H. L. Kuo, *Phys. Fluids* **6**, 195 (1963).
- <sup>2</sup>G. Schmidt, *Physics of High Temperature Plasmas*, 2nd ed. (Academic, New York, 1979), p. 126.
- <sup>3</sup>S. Goldstein, *Proc. R. Soc. London, Ser. A* **132**, 524 (1931).
- <sup>4</sup>E. L. Ruden, *IEEE Trans. Plasma Sci.* **30**, 611 (2002).
- <sup>5</sup>U. Shumlak and N. F. Roderick, *Phys. Plasmas* **5**, 2384 (1998).
- <sup>6</sup>G. I. Taylor, *Proc. R. Soc. London, Ser. A* **132**, 499 (1931).
- <sup>7</sup>S. Chandrasekhar, *Hydrodynamic and Hydromagnetic Stability* (Dover, New York, 1961), p. 434.
- <sup>8</sup>W. B. Thompson, *Rep. Prog. Phys.* **24**, 363 (1961).
- <sup>9</sup>K. V. Roberts and J. B. Taylor, *Phys. Rev. Lett.* **8**, 197 (1962).
- <sup>10</sup>R. D. Hazeltine and J. D. Meiss, *Plasma Confinement* (Addison-Wesley, Redwood, 1992).
- <sup>11</sup>M. Mathuthu, T. G. Zengen, and A. V. Gholap, *IEEE Trans. Plasma Sci.* **26**, 14 (1998).
- <sup>12</sup>G. Decker, W. Kies, and G. Pross, *Phys. Lett.* **89A**, 393 (1982).
- <sup>13</sup>J. V. Uspensky, *Theory of Equations* (McGraw-Hill, New York, 1948), p. 82.
- <sup>14</sup>W. H. Press, B. P. Flannery, S. A. Teukolsky, and W. T. Vetterling, *Numerical Recipes* (Cambridge University Press, New York, 1986), p. 263.
- <sup>15</sup>N. A. Krall and A. W. Trivelpiece, *Principles of Plasma Physics* (McGraw-Hill, New York, 1973), pp. 124–126.
- <sup>16</sup>H. Bruzzone and J. F. Martinez, *Plasma Sources Sci. Technol.* **10**, 471 (2001).
- <sup>17</sup>S. M. Gol'berg and A. L. Velikovich, *Phys. Fluids B* **5**, 1164 (1993).
- <sup>18</sup>D. D. Ryutov, M. S. Derzon, and M. K. Matzen, *Rev. Mod. Phys.* **72**, 167 (2000).
- <sup>19</sup>H. Knoepfel, *Pulsed High Magnetic Fields* (Elsevier, New York, 1970).
- <sup>20</sup>S. Lee and A. Serban, *IEEE Trans. Plasma Sci.* **24**, 1101 (1996).
- <sup>21</sup>M. Mitchner and R. K. Landshoff, *Phys. Fluids* **7**, 862 (1964).
- <sup>22</sup>T. P. Ray and A. I. Ershkovich, *Mon. Not. R. Astron. Soc.* **204**, 821 (1983).
- <sup>23</sup>J. D. Huba and D. Winske, *Phys. Plasmas* **5**, 2305 (1998).
- <sup>24</sup>J. D. Huba, *Phys. Rev. Lett.* **72**, 2033 (1994).
- <sup>25</sup>M. Scholz, R. Miklaszewski, M. Paduch, M. J. Sadowski, and K. Tomaszewski, *IEEE Trans. Plasma Sci.* **30**, 476 (2002).
- <sup>26</sup>M. N. Rosenbluth and A. Simon, *Phys. Fluids* **8**, 1300 (1965).
- <sup>27</sup>J. D. Huba, *Phys. Plasmas* **3**, 2523 (1996).
- <sup>28</sup>X. M. Qiu, L. Huang, and G. D. Jian, *Phys. Plasmas* **10**, 2956 (2003).
- <sup>29</sup>U. Shumlak, B. A. Nelson, R. P. Golingo, S. L. Jackson, E. A. Crawford, and D. J. Den Hartog, *Phys. Plasmas* **10**, 1683 (2003).